



Phase velocities from seismic noise using beamforming and cross correlation in Costa Rica and Nicaragua

Nicholas Harmon,¹ Peter Gerstoft,¹ Catherine A. Rychert,¹ Geoffrey A. Abers,² Mariela Salas de la Cruz,³ and Karen M. Fischer³

Received 17 July 2008; revised 15 August 2008; accepted 22 August 2008; published 3 October 2008.

[1] An expression for the cross correlation of noise between seismic stations and the 2D Green's function is derived assuming that noise travels as 2D surface waves. The phase velocity is obtained directly from the noise correlation function with a phase shift of $+\pi/4$. Mean phase velocity dispersion curves are calculated for the TUCAN seismic array in Costa Rica and Nicaragua from ambient seismic noise using two independent methods, noise cross correlation and beamforming. The noise cross correlation and beamforming methods are compared and contrasted by evaluating results from the TUCAN array. The results of the two methods as applied to the TUCAN array agree within 1%, giving good confidence in the phase velocities extracted from noise. **Citation:** Harmon, N., P. Gerstoft, C. A. Rychert, G. A. Abers, M. Salas de la Cruz, and K. M. Fischer (2008), Phase velocities from seismic noise using beamforming and cross correlation in Costa Rica and Nicaragua, *Geophys. Res. Lett.*, *35*, L19303, doi:10.1029/2008GL035387.

1. Introduction

[2] While group velocities are unambiguously retrieved from stacked noise cross correlation functions (NCFs) [Shapiro and Campillo, 2004], phase velocity estimation is not as straight forward [Yao *et al.*, 2006; Bensen *et al.*, 2007; Harmon *et al.*, 2007; Gouedard *et al.*, 2008; Lin *et al.*, 2008]. First, there is some ambiguity regarding which Green's function is extracted, i.e. whether the dimensionality of the noise distribution is 1D, 2D or 3D, leading to differences in the appropriate way to extract the Green's function. Second, 2D constructive interference from off great circle paths for a given station-to-station path can introduce a phase bias into the noise correlation function [Snieder, 2004]. Third, there is an integer cycle uncertainty in determining phase velocities from NCFs that typically requires prior information about phase velocities. This is usually determined from complimentary teleseismic surface wave studies.

[3] Seismic noise recorded at land-based seismic stations most likely travels as surface waves [Tanimoto, 2006; Webb, 2007]. Therefore, we develop the 2D model of noise distribution and the relationship between the noise correlation function and the Green's function. We present the

expected phase shift from constructive interference of isotropically distributed plane waves for the 2D model. Finally, the cycle ambiguity is determined in the typical method for the NCF phase velocity estimates by matching the phase velocities from teleseismic phase velocity studies. However, we demonstrate beamforming can successfully reproduce the mean phase velocity dispersion curve derived from the noise correlation function without the need for information from teleseismic surface wave studies by comparing NCF and beamforming results from the TUCAN array in Costa Rica and Nicaragua [Abers *et al.*, 2007]. The TUCAN array was not optimized for a surface wave study but, as we show, its array aperture and geometry are sufficient to validate the beamforming method.

2. Models of Ambient Seismic Noise

[4] For two seismic stations located in a 3D isotropic distribution of plane waves, the normalized cross spectral density function in the frequency domain is $R(\omega) = \sin(a)/a$, $a = \omega s/c$, (Figure 1a) where s is station separation and c is phase velocity [Cox, 1973]. In the time domain, using an inverse Fourier transform, this noise correlation function $R(t)$ is a boxcar function, $R(t) = H(t + s/c) - H(t - s/c)$ where H is the Heaviside step function (black line in Figure 1b). Thus, $\frac{dR(t)}{dt} \approx \delta(t + s/c) - \delta(t - s/c)$. The two terms correspond to the acausal minus the causal free-space Green's function. Thus, it has been suggested that the seismic Green's function, here theoretically a Dirac δ -function, can be extracted from noise correlation functions by taking the negative time derivative of the causal part of the cross correlation of the stations' time series [Roux *et al.*, 2005; Sabra *et al.*, 2005]. To recover the phase of a great circle path plane wave a phase shift of $\pi/2$ to the NCF is needed owing to the time derivative. In practice, often an additional phase shift of $-\pi/4$ is needed to account for the phase lag of a surface wave, though not needed by the 3D theory. This is because most microseisms travel as 2D surface waves [Tanimoto, 2006; Webb, 2007].

[5] The problem can be directly and self-consistently represented completely in 2D. A simple model for the noise correlation function, R , in the frequency domain for two stations with isotropically distributed plane waves in 2D is [Aki, 1957]:

$$R(\omega) = \int_{-\pi}^{\pi} A_0 e^{\frac{j\omega s \cos \theta}{c}} d\theta, \quad (1)$$

where θ is the azimuth with respect to the great circle path between the two stations and $A_0(\theta)$ is the amplitude of the

¹Scripps Institution of Oceanography, La Jolla, California, USA.

²Lamont-Doherty Earth Observatory, Earth Institute at Columbia University, Palisades, New York, USA.

³Geological Sciences, Brown University, Providence, Rhode Island, USA.

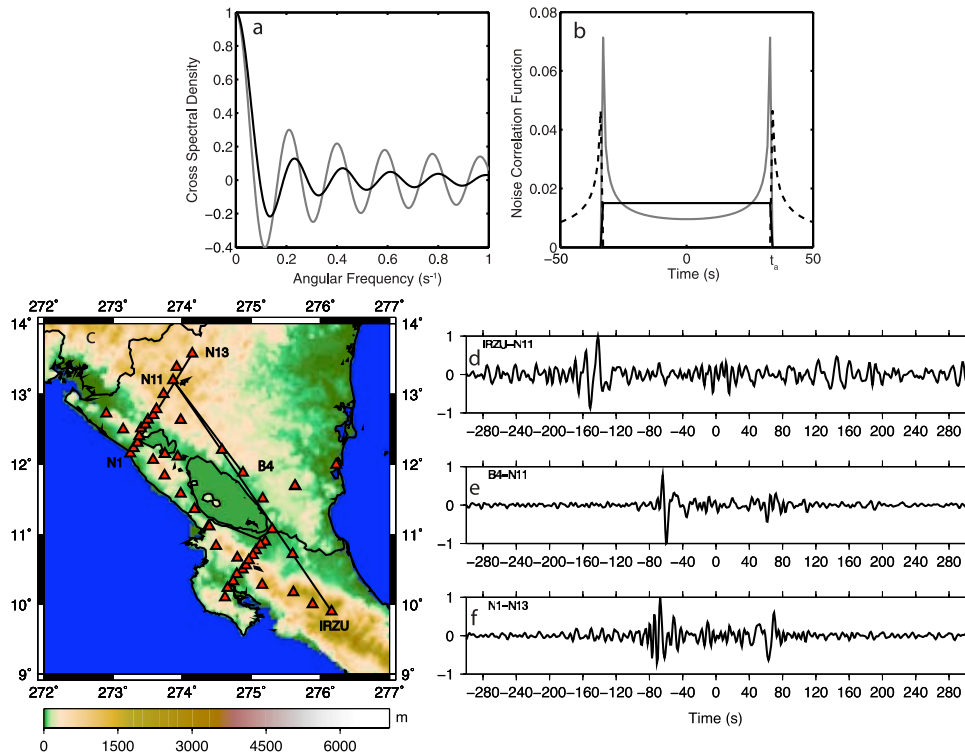


Figure 1. (a) Cross spectral density functions and (b) time domain correlation functions for 3D (black), 2D (gray) noise distribution of plane waves and the causal and acausal 2D Green's Function (dashed black). The travel time between the two stations is 33 s. (c) Station locations (red triangles) and topography (from ETOPO2) of the TUCAN array. The time series show the normalized bandpass filtered (5–33 s) NCF between stations (d) IRZU–N11, (e) B4–N11, and (f) N1–N13. Positive lags correspond to waves traveling from N11 and N13.

plane wave at each azimuth. A similar model could be obtained using point sources [Snieder, 2004].

[6] Integrating equation (1) assuming $A_0 = 1/2\pi$ yields a cross spectral density function $R(\omega) = J_0(\omega s/c)$ where J_0 is the zeroth-order Bessel function of the first kind [Aki, 1957]. The inverse Fourier transform of $J_0(\omega s/c)$, or the noise correlation function, is:

$$R(t) = \begin{cases} \frac{1}{\pi\sqrt{t_a^2 - t^2}} & \text{for } t \leq \frac{|s|}{c}, \\ 0 & \text{otherwise} \end{cases}, \quad (2)$$

where $t_a = s/c$ is the great axis arrival time.

[7] For a 2D medium, the Green's function, G , for a scalar wave equation is given by [Sanchez-Sesma and Campillo, 2006]:

$$G(\omega) = \frac{1}{4i\mu} H_0^{(2)}(\omega s/c) = \frac{1}{4i\mu} (J_0(\omega s/c) - iY_0(\omega s/c)), \quad (3)$$

where μ is the shear modulus and H_0 is the zeroth-order Hankel function of the second kind, and Y_0 is the zeroth order Bessel function of the second kind. In the time domain ($t \geq 0$)

$$G(t) = \begin{cases} \frac{1}{2\pi\mu\sqrt{t^2 - t_a^2}} & \text{for } t \geq \frac{s}{c} \\ 0 & \text{otherwise} \end{cases} \quad (4)$$

[8] In 2D, the NCF and Green's functions have a “tail” on the impulse (grey and black dashed lines, respectively in Figure 1b). The “tail” on the 2D Green's function extends to infinity, and results in a $+\pi/4$ phase shift for surface waves relative to a plane wave in the far field [Aki and Richards, 2002]. However, the “causal” NCF is used for determining phase velocity. For the one-sided causal noise correlation function R_c

$$R_c(\omega) = \int_{-\frac{\pi}{2}}^{\frac{\pi}{2}} A_0 e^{-i\omega s \frac{\cos \theta}{c}} d\theta \quad (5)$$

Rewriting the Hankel function [Abramowitz and Stegun, 1965]

$$H_0^{(2)}(z) = \frac{1}{\pi} \int_{-\pi/2}^{\pi/2} \exp(iz \cos \theta) d\theta + \frac{2i}{\pi} \int_0^{\infty} \exp(-z \sinh \phi) d\phi \quad (6)$$

into equation (5) gives ($A_0 = 1/2\pi$)

$$R_c(\omega) = \frac{1}{2} H_0^{(2)}\left(\frac{\omega s}{c}\right) - \frac{i}{\pi} \int_0^{\infty} \exp\left(-\frac{\omega s}{c} \sinh \phi\right) d\phi \\ \approx \frac{1}{2} H_0^{(2)}\left(\frac{\omega s}{c}\right) - \frac{i}{\pi} \left(\frac{c}{\omega s} - \left(\frac{c}{\omega s}\right)^3 \dots\right) \quad (7)$$

[9] From equation (7), $R_c(\omega)$ is proportional to $iG(\omega)$ plus an imaginary-valued power series similar to *Sanchez-Sesma and Campillo* [2006]. The power series decays faster than the Hankel function so that in the far field, the NCF gives a $-\pi/4$ phase shift relative to a great circle path plane wave. To correct the NCF to the Green's function (multiplication by i in frequency domain) gives a $+\pi/2$ phase shift. The phase shift from the far field Green's function to a great circle path plane wave is $-\pi/4$. Thus, the total phase shift is $\pi/2 - \pi/4 = +\pi/4$ to correct the causal NCF to the great circle path plane wave. Note, that approaches that take the time derivative [*Yao et al.*, 2006, *Lin et al.*, 2008], multiplying with $i\omega$ in frequency domain (a $+\pi/2$ shift), and then apply the $-\pi/4$ phase shift result in the same correction.

3. Phase Velocity From NCF

[10] We determined phase velocities using 593 days (July 2004 to March 2006) of station to station NCF for the vertical components of the 49 stations of the TUCAN seismic array (Figure 1c) using a method similar to *Harmon et al.* [2007]. Variations from *Harmon et al.* [2007] include removing the instrument responses from the signals (TUCAN contains different sensor types), decimation to 1 s sampling, a RMS clipping scheme for the daily time series [*Sabra et al.*, 2005] and signal whitening by normalizing the Fourier coefficients by their respective magnitude, both to create a single broadband NCF. Then we cross correlated hourly time series segments for all station pairs and stacked the resulting correlograms. The NCF phase dispersion was determined by unwrapping the phase of the stacked NCF and applying a $\pi/4$ correction. We determined the cycle ambiguity by matching the average phase velocity determined from teleseismic events at 20 s period. The mean teleseismic phase velocity estimates were determined using the method of *Yang and Forsyth* [2006], with 95 events with good azimuthal coverage. We calculate the mean phase dispersion curve and its standard error of the mean by station-to-station distance-weighted averaging. A station-to-station NCF phase velocity estimate was used to calculate the mean phase dispersion curve if 1) the NCF had signal to noise ratio >10 , 2) the average of the phase velocity from all the ~ 4 month NCF stacks had a standard deviation of <0.1 km/s and 3) the station-to-station path was greater than 3λ after *Lin et al.* [2008]. Distance weighting was chosen since longer paths should be more representative of average structure. For 15–29 s periods, the teleseismic and NCF mean phase velocity estimates were within 1%, except at 18 s where they were within 2%.

4. Phase Velocity From Beamforming

[11] The beamforming method inverts the phase information from a seismic array for short time series for the best fitting phase slowness and back azimuth of a plane wave. The beamforming method uses the spatial correlation at all stations of the phase information with a given plane wave to find the average phase velocity within the array. In contrast, phase velocity estimates from the NCF determine the phase delay between individual station pairs of a known distance from long time series. The NCF requires time periods of several days or longer to generate reasonable estimates of

the noise distribution [*Stehly et al.*, 2006] while the beamforming method can resolve phase velocity and source azimuth on time scales as short as 10 min. [*Gerstoft et al.*, 2006].

[12] Beamforming was performed following *Gerstoft et al.* [2006] and *Gerstoft and Tanimoto* [2007]. The data for each day was split into 512-s time series, which were then clipped, normalized, and Fourier transformed. For each frequency, we kept the phase of the signal. At each frequency, we estimated a complex-valued vector $\mathbf{v}(\omega, t_i)$ containing the response from the 49 stations used in the TUCAN array, where t_i refers to the start time of the Fourier transform.

[13] The cross-spectral density matrix \mathbf{C} is given by $\langle \mathbf{v}\mathbf{v}^T \rangle$, where the brackets indicate temporal averaging over all t_i for each day. The plane wave response for the seismic array is given by $\mathbf{p}(\omega, c, \theta, \mathbf{r}) = \exp(i\omega(\mathbf{r}\mathbf{e})/c)$, where \mathbf{r} describes the coordinates of the array relative to the mean coordinates and \mathbf{e} contains the directional cosines of the plane wave. The beamformer output is given by: $\mathbf{b}(\omega, c, \theta, t) = \mathbf{p}(\omega, c, \theta)^T \mathbf{C}(\omega, t) \mathbf{p}(\omega, c, \theta)$.

[14] We searched for the maximum beamformer output, corresponding to the best fitting plane wave, over slowness ($1/c$) from 0.00–0.40 s/km ($2.5-\infty$ km/s) and every 2° from 0– 360° azimuth for each day. To calculate the mean phase velocity dispersion curve we determine the velocity corresponding to the maximum beamformer output for each day and period, and use the beamformer output as the weights for the average and the weighted standard error of the mean.

5. Results and Discussion

[15] For station-to-station paths perpendicular to the Pacific coast, the NCFs are dominated by 6–10 s microseisms coming from the coast. This can be seen by comparing NCFs with comparable path lengths and different orientations such as N1–N13 and B4–N11 (Figures 1f and 1e). A high frequency signal owing to the Pacific microseisms is seen at negative lag (from southwest) for the path perpendicular to the Pacific coast whereas no high frequency signal is seen at positive lag for this path (Figure 1f) or for positive and negative lags of the coast parallel paths (Figures 1d and 1e). The amplitudes and frequency contents of the NCFs suggest that the noise distribution changes with period.

[16] For periods between 10–22 s, the beamformer output in Figure 2a there is a nearly continuous ring maximum with surface wave slownesses, suggesting surface waves dominate the signal in this period range, which is consistent with the 2D model of noise distribution. If the noise were distributed uniformly in the Earth (3D assumption) with no beamformer aliasing, we would expect to see a maximum in the beamformer output at all azimuths and for all slownesses from 0.00 s/km to the best fitting slowness of a surface wave (Figure 2a). Above 18 s period there is little signal from the Pacific ($180-240^\circ$), while in the secondary microseism band (6–10 s period) the dominant source direction is $180-240^\circ$ azimuth with little energy coming from other directions, which is consistent with what was observed in the NCF. Point sources may contribute to the apparent azimuthal coverage by smearing energy across

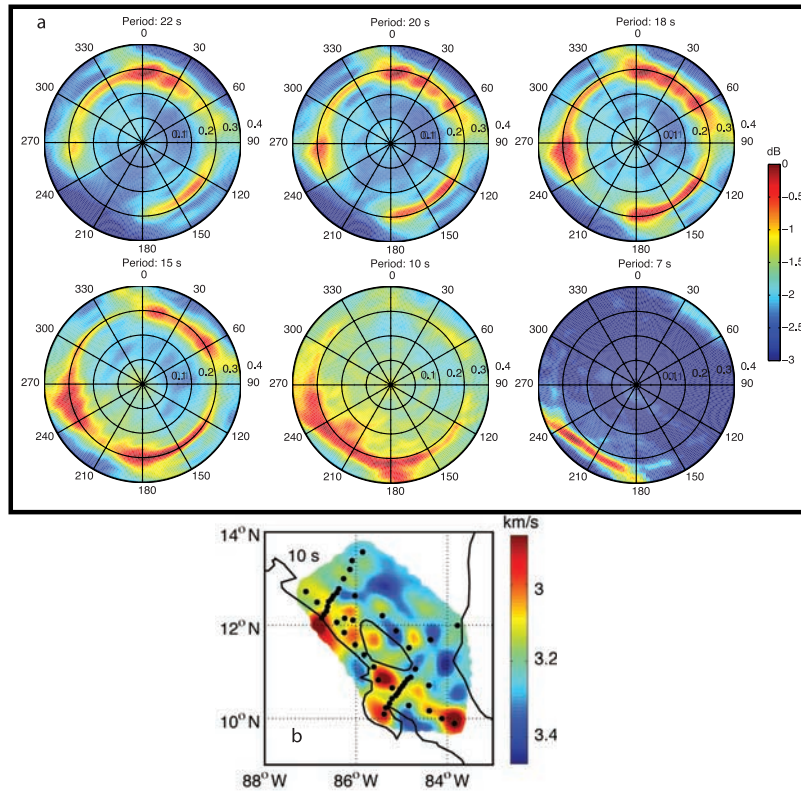


Figure 2. (a) Azimuth vs. phase slowness plots of 593-day stack of beamformer output (dB) of the TUCAN array for 7, 10, 15, 18, 20 and 22 s period. Slowness is the radial distance on the polar plots from 0.00–0.4 s/km. (b) Velocity model for 10 s period NCF with station locations (circles).

azimuths, but have little effect on the accuracy of the beamformer phase velocities. Although not possible here, azimuthal anisotropy might be recovered from the beamformer output.

[17] For periods greater than 6 s, both NCF and beamformer average phase velocity estimates are within error of each other (Figure 3). For the best-resolved periods (7–20 s), the phase velocity from beamforming agrees within 1% with the NCF estimates. The agreement is best in this band because this is where the microseisms are strongest (see Figure 2a). Below 6 s period, the agreement between the two estimates begins to erode due to aliasing as the beamformer output no longer resolves any coherent surface waves and the errors in the NCF estimates increase. The NCF estimate is more stable due to the inherent averaging in the frequency domain caused by windowing in the time domain. Note, that the errors statistics for beamforming are based on all data, whereas the NCF are based on the best data.

[18] The station geometry requirements for the two methods are different. The NCF method requires only 2 stations. Beamforming, on the other hand, requires an array of stations. We choose NCF station spacing to be at least 3λ at 20 s period to avoid near field effects and to allow distinct phases to emerge [Bensen et al., 2007]. Data selection requirements of the NCF limit the number of station pairs to 270 out of 1149 at 20 s. For beamforming array aperture larger than 1λ is required to resolve the longest periods of interest and station spacing $< \lambda/2$ to

prevent spatial aliasing at shortest periods for a regularly spaced array, but for irregular arrays it can be relaxed somewhat. For the TUCAN array which consists mainly of two regularly-spaced line arrays pointing southwest,

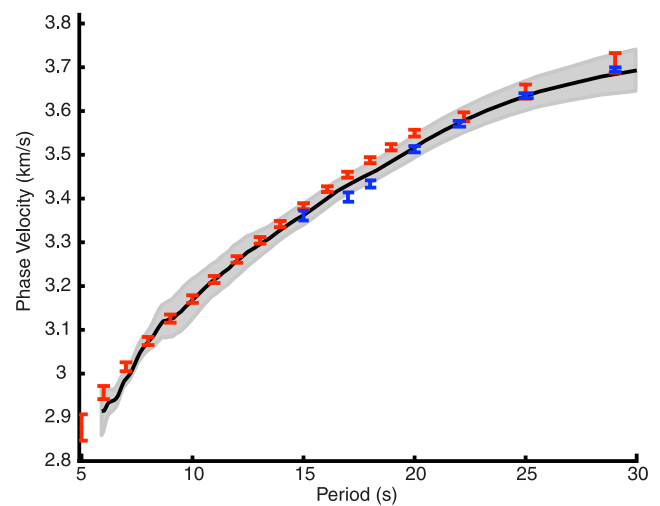


Figure 3. Phase velocity estimates from beamforming (solid black line) with $3\times$ standard error of the mean (grey region), noise correlation methods (circles) with $3\times$ standard error of the mean bars and teleseismic phase velocity estimates (open squares) with $3\times$ standard error of the mean.

beamforming aliasing manifests itself as a straight-line beamformer output (perpendicular to the line array directions) rather than a point for sources coming from the southwest, as shown in the 7 s band in Figure 2a. For shorter periods, the beamformer aliasing becomes more severe making it difficult to extract phase velocities. In the 7–20 s bands, the phase slowness can be resolved but aliasing does contribute to the errors in the phase slowness estimates. Overall, the aliasing at the periods of interest, 7–20 s, is minor while it dominates at periods less than 7 s.

[19] Additional sources of error in the average phase velocity estimates include measurement error of the phase, heterogeneous earth structure and heterogeneous source distribution. Measurement error for both methods is smaller at short periods owing to the shorter time length of the phase. Errors due to earth structure can be assessed through the reduction of the variance from tomographic inversion of the NCF phase velocities for 2D velocity structure. At 10 s period (Figure 2b), our velocity model has maximum heterogeneities of $\pm 10\%$ of the mean of 3.17 km/s, resulting in a 78% variance reduction of the data.

[20] To assess error due to heterogeneous structure and source distribution in the beamformer estimates we calculated the predicted beamformer output for the 2D NCF phase velocity model at 10 s period (Figure 2b) assuming a uniform velocity (3.17 km/s) outside the array for distant events (>5000 km) with $0\text{--}360^\circ$ back azimuths. We use the 2D Rayleigh phase sensitivity kernels of Zhou *et al.* [2004] to calculate the predicted phase for the model. For all azimuths, best fitting phase velocities are within 2% of the uniform velocity. While for a narrow range of back azimuths, like Figure 2a, 7 s period, the velocities are within 1%, mirroring the decrease in the beamformer errors we observe below 9 s period. Beamformer estimates are stable (Figure 3) since they represent a wave propagation average across the entire array. At 10 s in Figure 2a, the peak is resolvable but broader compared to longer periods, which could be a result of decorrelation owing to velocity heterogeneity or less microseism energy at that period. This broadening contributes to the slight increase in error for the beamformer estimates for the 9–14 s periods in Figure 3.

[21] Heterogeneous noise distributions can create a systematic error in the phase velocity estimate requiring a phase shift other than $\pi/4$ for the NCF, which may explain some of the difference between the NCF and teleseismic estimates. Therefore, the quality of the phase velocity estimates for both methods should be considered in conjunction with the noise distribution. Similarly, the noise distribution might be useful for empirically determining the correct phase shift for the NCF.

6. Conclusions

[22] 1. We derive a relationship between the NCF and 2D Green's function for a 2D noise distribution and show that extraction of unbiased phase velocities from the NCF requires a $\pi/4$ phase shift. The good agreement between the NCF beamformer and teleseismic velocities suggests to first order that our model holds for real earth structure.

[23] 2. Beamformer output provides valuable information about noise distribution through time. We show that from

7–20 s period seismic noise in clipped seismograms for 18 months of data is dominated by surface waves and is consistent with a 2D model of noise distribution, having good azimuthal coverage from 10–22 s period.

[24] 3. Beamforming provides an accurate, independent estimate of the mean phase velocity dispersion across a seismic array that is within 1% of NCF and teleseismic estimates. Thus, beamforming can potentially resolve the cycle ambiguity in NCF phase velocity estimates without a complimentary teleseismic study.

[25] **Acknowledgments.** N. Harmon is supported by NSF OCE 0622932 and P. Gerstoft is supported by the US Air Force, FA8718-07-C-0005. We thank D. W. Forsyth and G. Masters for useful discussions.

References

- Abers, G. A., K. M. Fischer, M. Protti, and W. Strauch (2007), The TUCAN broadband seismometer experiment: Probing mantle melting in the Nicaragua–Costa Rica Subduction Zone, *IRIS Newsl.*, 1, 10–12.
- Abramowitz, M., and I. Stegun (Eds.) (1965), *Handbook of Mathematical Functions, With Formulas, Graphs, and Mathematical Tables*, Dover, New York.
- Aki, K. (1957), Space and time spectra of stationary and stochastic waves, with special reference to microtremors, *Bull. Earthquake Res. Inst.*, 35, 415–457.
- Aki, K., and P. G. Richards (2002), *Quantitative Seismology*, Univ. Sci., Sausalito, Calif.
- Bensen, G. D., M. H. Ritzwoller, M. P. Barmin, A. L. Levshin, F. Lin, M. P. Moschetti, N. M. Shapiro, and Y. Yang (2007), Processing seismic ambient noise data to obtain reliable broad-band surface wave dispersion measurements, *Geophys. J. Int.*, 169, 1239–1260, doi:10.1111/j.1365-1246X.2007.03374.x.
- Cox, H. (1973), Spatial correlation in arbitrary noise fields with application to ambient sea noise, *J. Acoust. Soc. Am.*, 54(5), 1289–1301.
- Gerstoft, P., and T. Tanimoto (2007), A year of microseisms in southern California, *Geophys. Res. Lett.*, 34, L20304, doi:10.1029/2007GL031091.
- Gerstoft, P., M. C. Fehler, and K. G. Sabra (2006), When Katrina hit California, *Geophys. Res. Lett.*, 33, L17308, doi:10.1029/2006GL027270.
- Gouedard, P., C. Cornou, and P. Roux (2008), Phase-velocity dispersion curves and small-scale geophysics using noise correlation slantstack technique, *Geophys. J. Int.*, 172, 971–981, doi:10.1111/j.1365-1246X.2007.03654.x.
- Harmon, N., D. Forsyth, and S. Webb (2007), Using ambient seismic noise to determine short-period phase velocities and shallow shear velocities in young oceanic lithosphere, *Bull. Seismol. Soc. Am.*, 97, 2024–2039.
- Lin, F., M. P. Moschetti, and M. H. Ritzwoller (2008), Surface wave tomography of the western United States from ambient seismic noise: Rayleigh and Love wave phase velocity maps, *Geophys. J. Int.*, 173, 281–298, doi:10.1111/j.1365-1246X.2008.03720.x.
- Roux, P., K. G. Sabra, W. A. Kuperman, and A. Roux (2005), Ambient noise cross correlation in free space: Theoretical approach, *J. Acoust. Soc. Am.*, 117(1), 79–84.
- Sabra, K. G., P. Gerstoft, P. Roux, W. A. Kuperman, and M. C. Fehler (2005), Extracting time-domain Green's function estimates from ambient seismic noise, *Geophys. Res. Lett.*, 32, L03310, doi:10.1029/2004GL021862.
- Sanchez-Sesma, F. J., and M. Campillo (2006), Retrieval of the green's function from cross correlation: The canonical elastic problem, *Bull. Seismol. Soc. Am.*, 96, 1182–1191.
- Shapiro, N. M., and M. Campillo (2004), Emergence of broadband Rayleigh waves from correlations of the ambient seismic noise, *Geophys. Res. Lett.*, 31, L07614, doi:10.1029/2004GL019491.
- Snieder, R. (2004), Extracting the Green's function from the correlation of coda waves: A derivation based on stationary phase, *Phys. Rev. E*, 69(4), 046610, doi:10.1103/PhysRevE.1169.046610.
- Stehly, L., M. Campillo, and N. M. Shapiro (2006), A study of the seismic noise from its long-range correlation properties, *J. Geophys. Res.*, 111, B10306, doi:10.1029/2005JB004237.
- Tanimoto, T. (2006), Excitation of normal modes by nonlinear interaction of ocean waves, *Geophys. J. Int.*, 168, 571–582, doi:10.1111/j.1365-1246X.2006.03240.x.
- Webb, S. C. (2007), The Earth's 'hum' is driven by ocean waves over the continental shelves, *Nature*, 445(7129), 754–756.

- Yang, Y., and D. W. Forsyth (2006), Regional tomographic inversion of amplitude and phase of Rayleigh waves with 2-D sensitivity kernels, *Geophys. J. Int.*, *166*, 1148–1160.
- Yao, H., R. D. Van der Hilst, and M. V. De Hoop (2006), Surface-wave array tomography in SE Tibet from ambient seismic noise and two-station analysis: I - Phase velocity maps, *Geophys. J. Int.*, *166*, 732–744, doi:710.1111/j.1365-1246X.2006.03028.x.
- Zhou, Y., F. A. Dahlen, and G. Nolet (2004), Three-dimensional sensitivity kernels for surface wave observables, *Geophys. J. Int.*, *158*, 142–168.
-
- P. Gerstoft, N. Harmon, and C. A. Rychert, Scripps Institution of Oceanography, 9500 Gilman Drive, MC 0225, La Jolla, CA 92093-0225, USA. (nharmon@ucsd.edu)
- G. A. Abers, Lamont-Doherty Earth Observatory, Earth Institute at Columbia University, 61 Route 9W, Palisades, NY 10964, USA.
- K. M. Fischer and M. Salas de la Cruz, Geological Sciences, Brown University, 325 Brook Street, Providence, RI 02912, USA.